Available online at www.sciencedirect.com
ScienceDirect
Comput. Methods Appl. Mech. Engrg. 305 (2016) 759–776
Computer methods in applied mechanics and engineering
www.elsevier.com/locate/cma

On the computational efficiency of the error estimator for Guyan reduction

Jin-Gyun Kim[a], Seung-Hwan Boo[b], Chang-Ock Lee[c], Phill-Seung Lee[b,*]

[a] *Mechanical Systems Safety Research Division, Korea Institute of Machinery and Materials, Daejeon, 34103, Republic of Korea*
[b] *Department of Mechanical Engineering, Korea Advanced Institute of Science and Technology, Daejeon, 34141, Republic of Korea*
[c] *Department of Mathematical Sciences, Korea Advanced Institute of Science and Technology, Daejeon, 34141, Republic of Korea*

Received 9 June 2015; received in revised form 22 February 2016; accepted 19 March 2016
Available online 28 March 2016

Abstract

An improved error estimator for Guyan reduction is presented for efficient calculation of the relative eigenvalue error. In this work, the original error estimator is simply redefined in the level of the component matrix by neglecting its component matrices that do not affect the performance of estimation. Consequently, a new simple formulation of the error estimator is developed. Compared with the original formulation, it leads to better computational efficiency without significant loss of the estimating accuracy. The performance of the present error estimator is demonstrated theoretically and numerically.

Keywords: Error estimation; Guyan reduction; Reduced order modeling; Finite element method; Structural dynamics; Eigenvalue problem

1. Introduction

The dynamic response of the large finite element (FE) model is often approximated using reduced-order modeling techniques due to their computational efficiency [1–21]. In particular, dynamic condensation methods such as Guyan reduction and the IRS (Improved reduced system) method have been widely used for numerical–experimental model correlation, active vibration control, FE model updating, and parameter identification [1–9].

A major drawback of dynamic condensation methods was lack of an efficient error estimation technique to evaluate the reliability of the reduced model [22]. However, a novel error estimator was recently developed to accurately predict the relative eigenvalue error without the original eigenvalue, and its excellent performance was also verified with various numerical examples [23]. Because the error estimator is calculated using simple additions and multiplications of known matrices and vectors, its computational cost might be low. However, when the size of the original FE model is large, those matrix operation costs also become quite significant. Furthermore, due to its complicated formulation, there are lots of difficulties to extend it for the IRS method [5] and model reduction in non-classical damping systems.

* Corresponding author.
E-mail address: phillseung@kaist.edu (P.-S. Lee).

http://dx.doi.org/10.1016/j.cma.2016.03.030
0045-7825/

To handle this problem, in this study, the original formulation of the error estimator is explored at the component matrix level, and we find which component matrices disappear or have minor effect in the error estimator. Consequently, we are able to derive a much simpler formulation of the error estimator. To verify this computational efficiency, we also study the specific operation counts of the original and present formulations.

In the following section, we first revisit Guyan reduction. In Section 3, the original error estimator is derived again from the new point of view, and its characteristics are studied. In Section 4, we newly propose a well-defined formulation of the original error estimator, and then its performance is tested using various numerical examples in Section 5. The conclusions are given in Section 6.

2. Guyan reduction

In Guyan reduction [1], the original eigenvalue problem can be written

$$\mathbf{K}\mathbf{u} = \lambda\mathbf{M}\mathbf{u}, \quad \mathbf{u} = \mathbf{\Phi}\mathbf{q}, \tag{1}$$

with

$$\mathbf{M} = \begin{bmatrix} \mathbf{M}_{11} & \mathbf{M}_{12} \\ \mathbf{M}_{21} & \mathbf{M}_{22} \end{bmatrix}, \qquad \mathbf{K} = \begin{bmatrix} \mathbf{K}_{11} & \mathbf{K}_{12} \\ \mathbf{K}_{21} & \mathbf{K}_{22} \end{bmatrix}, \qquad \mathbf{u} = \begin{bmatrix} \mathbf{u}_1 \\ \mathbf{u}_2 \end{bmatrix}, \tag{2}$$

where $\mathbf{M}$ and $\mathbf{K}$ are the mass and stiffness matrices of the original FE model, respectively, $\mathbf{u}$ is the displacement vector, and λ is the original eigenvalue. Here, $\mathbf{\Phi}$ and $\mathbf{q}$ are the original eigenvector matrix and generalized coordinate vector, respectively. In structural models, $\mathbf{M}$ and $\mathbf{K}$ are $N \times N$ positive or semi-positive definite matrices. Here, N is the number of degrees of freedom (DOFs) in the original model. Subscripts 1 and 2 denote "master" and "slave" DOFs, which mean dominant and residual DOFs [1,2]. Generally, the number of master DOFs, N_1, is a small portion of total DOFs ($N_1 \ll N_2 < N$), and N_2 is the number of slave DOFs ($N = N_1 + N_2$). Master DOFs are only retained in the final reduced model.

From the second row in Eq. (1), $\mathbf{u}_2$ is expressed as

$$\mathbf{u}_2 = [\mathbf{K}_{22} - \lambda\,\mathbf{M}_{22}]^{-1}\,[\lambda\,\mathbf{M}_{21} - \mathbf{K}_{21}]\,\mathbf{u}_1, \tag{3}$$

and then, the inverse of $[\mathbf{K}_{22} - \lambda\,\mathbf{M}_{22}]$ can be expanded as

$$[\mathbf{K}_{22} - \lambda\,\mathbf{M}_{22}]^{-1} = \mathbf{K}_{22}^{-1} + \lambda\mathbf{K}_{22}^{-1}\mathbf{M}_{22}\mathbf{K}_{22}^{-1} + O\left(\lambda^2\right) + O\left(\lambda^3\right) + \cdots. \tag{4}$$

Note that the expansion in Eq. (4) is valid if the eigenvalue λ is smaller than the smallest eigenvalue σ_1 obtained from the eigenvalue problem $[\mathbf{K}_{22} - \sigma_i\mathbf{M}_{22}]\,\boldsymbol{\psi}_i = \mathbf{0}$ [24–26]. In Guyan reduction, this condition is generally satisfied because master DOFs are selected to reflect lower modes of the original FE model well [25].

Neglecting the higher order terms of λ (more than 2nd order) in Eq. (4) and substituting it into Eq. (3), we have

$$\mathbf{u}_2 = [\mathbf{K}_{22}^{-1} + \lambda\mathbf{K}_{22}^{-1}\mathbf{M}_{22}\mathbf{K}_{22}^{-1}][\lambda\mathbf{M}_{21} - \mathbf{K}_{21}]\mathbf{u}_1. \tag{5}$$

Using Eq. (5), the displacement vector $\mathbf{u}$ can be approximated as

$$\mathbf{u} \approx \bar{\mathbf{u}} = \mathbf{T}_K\,\mathbf{u}_1, \qquad \mathbf{T}_K = \begin{bmatrix} \mathbf{I} \\ \left[\mathbf{K}_{22}^{-1} + \lambda\mathbf{K}_{22}^{-1}\mathbf{M}_{22}\mathbf{K}_{22}^{-1}\right]\,[\lambda\,\mathbf{M}_{21} - \mathbf{K}_{21}] \end{bmatrix}, \tag{6}$$

in which $\bar{\mathbf{u}}$ is the approximated displacement vector, and $\mathbf{T}_K$ was named as Kidder's transformation matrix [3]. Here, an overbar $\overline{(\cdot)}$ denotes approximated quantities.

In Guyan reduction, its transformation matrix denoted by $\mathbf{T}_G$ is defined from $\mathbf{T}_K$ without considering λ and λ^2 terms, and then the reduced matrices are calculated

$$\mathbf{M}_1 = \mathbf{T}_G^T\mathbf{M}\mathbf{T}_G, \qquad \mathbf{K}_1 = \mathbf{T}_G^T\mathbf{K}\mathbf{T}_G, \quad \text{and} \quad \mathbf{T}_G = \begin{bmatrix} \mathbf{I} \\ -\mathbf{K}_{22}^{-1}\,\mathbf{K}_{21} \end{bmatrix}, \tag{7}$$

where $\mathbf{M}_1$ and $\mathbf{K}_1$ are reduced mass and stiffness matrices, respectively, and its eigenvalue problem can be written

$$\mathbf{K}_1\mathbf{u}_1 = \bar{\lambda}\mathbf{M}_1\mathbf{u}_1, \quad \mathbf{u}_1 = \mathbf{\Phi}_1\mathbf{q}_1, \tag{8}$$

where $\bar{\lambda}$ is the approximated eigenvalue, and $\mathbf{\Phi}_1$ and $\mathbf{q}_1$ are the eigenvector matrix and generalized coordinate vector in the reduced model, respectively.

Here, $\mathbf{T}_K$ can be rewritten by the sum of the Guyan's transformation matrix $\mathbf{T}_G$ and the residual transformation matrix $\mathbf{T}_r$ as

$$\mathbf{T}_K = \mathbf{T}_G + \mathbf{T}_r, \quad \mathbf{T}_r = \lambda\,\mathbf{T}_r^{(1)} + \lambda^2\,\mathbf{T}_r^{(2)} \tag{9a}$$

with

$$\mathbf{T}_r^{(1)} = \begin{bmatrix} \mathbf{0} \\ \mathbf{K}_{22}^{-1}\mathbf{M}_{21} - \mathbf{K}_{22}^{-1}\mathbf{M}_{22}\mathbf{K}_{22}^{-1}\mathbf{K}_{21} \end{bmatrix}, \qquad \mathbf{T}_r^{(2)} = \begin{bmatrix} \mathbf{0} \\ \mathbf{K}_{22}^{-1}\mathbf{M}_{22}\mathbf{K}_{22}^{-1}\,\mathbf{M}_{21} \end{bmatrix}, \tag{9b}$$

where $\mathbf{T}_r^{(1)}$ and $\mathbf{T}_r^{(2)}$ are λ and λ^2 terms of the residual transformation matrix, respectively. Due to these compensations, the ith original eigenvector $(\boldsymbol{\varphi})_i$ is approximated more accurately in Kidder's approach than in the original Guyan reduction as

$$(\boldsymbol{\varphi})_i \approx (\bar{\boldsymbol{\varphi}})_i = \mathbf{T}_K(\boldsymbol{\varphi}_1)_i = (\mathbf{T}_G + \mathbf{T}_r)\,(\boldsymbol{\varphi}_1)_i. \tag{10}$$

It is also important to note that, since $\mathbf{T}_r^{(2)}$ is a higher order term of λ, it could be neglected for computational efficiency. This feature will be used to simplify the original formulation of the error estimator in Section 4.

3. Error estimator for Guyan reduction

In Guyan reduction, the accuracy of approximated eigenvalues calculated in Eq. (8) is generally evaluated as

$$\xi_i = \frac{\bar{\lambda}_i}{\lambda_i} - 1, \tag{11}$$

where ξ_i denotes the ith relative eigenvalue error. However, Eq. (11) is impractical because the original eigenvalue λ_i is calculated in the original eigenvalue problem.

To solve this problem, a novel technique was recently proposed to precisely estimate the relative eigenvalue error of Guyan reduction without the original eigenvalue λ_i [23]. In this section, we briefly review the derivation procedure of the error estimator.

The original eigenvalue problem in Eq. (1) could be rewritten as

$$\frac{1}{\lambda_i}(\boldsymbol{\varphi})_i^T\mathbf{K}(\boldsymbol{\varphi})_i = (\boldsymbol{\varphi})_i^T\mathbf{M}(\boldsymbol{\varphi})_i. \tag{12}$$

The original eigenvalue λ_i and the original eigenvector $(\boldsymbol{\varphi})_i$ can be presented as

$$\lambda_i = \bar{\lambda}_i - \delta\lambda_i, \tag{13a}$$

$$(\boldsymbol{\varphi})_i = (\bar{\boldsymbol{\varphi}})_i + (\delta\boldsymbol{\varphi})_i, \tag{13b}$$

in which $\delta\lambda_i$ and $(\delta\boldsymbol{\varphi})_i$ are error terms of eigenvalue and eigenvector, respectively. Note that the approximated eigenvalue $\bar{\lambda}_i$ is bigger than the original eigenvalue λ_i in general, and thus $\delta\lambda_i$ is a positive value in Guyan reduction ($\bar{\lambda}_i \geq \lambda_i$ and $\delta\lambda_i \geq 0$), see Refs. [26–29].

Substituting Eq. (13b) into Eq. (12), we have

$$\frac{1}{\lambda_i}(\bar{\boldsymbol{\varphi}})_i^T\mathbf{K}(\bar{\boldsymbol{\varphi}})_i - (\bar{\boldsymbol{\varphi}})_i^T\mathbf{M}(\bar{\boldsymbol{\varphi}})_i - \frac{1}{\lambda_i}(\delta\boldsymbol{\varphi})_i^T\mathbf{K}(\delta\boldsymbol{\varphi})_i + (\delta\boldsymbol{\varphi})_i^T\mathbf{M}(\delta\boldsymbol{\varphi})_i = 0, \tag{14}$$

and then, expanding Eq. (14) considering Eq. (10), the following equation is obtained

$$\frac{\bar{\lambda}_i}{\lambda_i} - 1 = \mathit{\Pi}(\lambda_i) + \delta\,\mathit{\Pi}\,(\lambda_i) \tag{15a}$$

with

$$\Pi(\lambda_i) = (\boldsymbol{\varphi}_1)_i^T [2\mathbf{T}_G + \lambda_i \mathbf{T}_r^{(1)} + \lambda_i^2 \mathbf{T}_r^{(2)}]^T [\lambda_i \mathbf{M} - \mathbf{K}][\mathbf{T}_r^{(1)} + \lambda_i \mathbf{T}_r^{(2)}](\boldsymbol{\varphi}_1)_i, \tag{15b}$$

$$\delta\Pi(\lambda_i) = (\delta\boldsymbol{\varphi})_i^T \left[\frac{1}{\lambda_i}\mathbf{K} - \mathbf{M}\right] (\delta\boldsymbol{\varphi})_i, \tag{15c}$$

in which the left-hand side in Eq. (15a) is the relative eigenvalue error in Eq. (11). Hence, in Eq. (15), the relative eigenvalue error is described as two functions of λ_i.

When the approximated eigensolutions are close enough to the exact original eigensolutions (that is, $\lambda_i \approx \bar{\lambda}_i$ and $(\boldsymbol{\varphi})_i \approx (\bar{\boldsymbol{\varphi}})_i$), it is possible to assume that

$$\Pi(\lambda_i) \approx \Pi(\bar{\lambda}_i), \quad \Pi(\bar{\lambda}_i) \gg \delta\Pi(\bar{\lambda}_i). \tag{16}$$

Then, using $\bar{\lambda}_i$ instead of λ_i in Eq. (15a) and neglecting $\delta\Pi(\bar{\lambda}_i)$, the relative eigenvalue could be approximated as

$$\frac{\bar{\lambda}_i}{\lambda_i} - 1 \approx \Pi(\bar{\lambda}_i). \tag{17}$$

Finally, using $\Pi(\bar{\lambda}_i)$ in Eq. (17), an error estimator η_i for the ith relative eigenvalue was defined as

$$\eta_i = (\boldsymbol{\varphi}_1)_i^T [2\mathbf{T}_G + \bar{\lambda}_i \mathbf{T}_r^{(1)} + \bar{\lambda}_i^2 \mathbf{T}_r^{(2)}]^T [\bar{\lambda}_i \mathbf{M} - \mathbf{K}] [\mathbf{T}_r^{(1)} + \bar{\lambda}_i \mathbf{T}_r^{(2)}](\boldsymbol{\varphi}_1)_i. \tag{18}$$

Its performance was demonstrated using various numerical examples, and also the computational efficiency was briefly investigated in the previous study in Ref. [23].

In addition, the error estimator is neither upper nor lower bounds of the exact error. To develop the error estimator, the approximated eigenvalue $\bar{\lambda}_i$ was used on the right-hand side in Eq. (15a) instead of the original eigenvalue λ_i, which is an unknown value. Then, the following relation is obtained

$$\Pi(\lambda_i) + \delta\Pi(\lambda_i) \approx \Pi(\bar{\lambda}_i) + \delta\Pi\left(\bar{\lambda}_i\right). \tag{19}$$

Then, $\Pi(\lambda_i)$ is a polynomial of λ_i, but $\delta\Pi(\lambda_i)$ is a fractional function of λ_i. Therefore, we have

$$\Pi(\lambda_i) \leq \Pi(\bar{\lambda}_i), \qquad \delta\Pi(\lambda_i) \geq \delta\Pi\left(\bar{\lambda}_i\right). \tag{20}$$

For this reason, it could not be theoretically verified whether the proposed error estimator η_i is an upper or lower bound of the relative eigenvalue error ξ_i.

It is important to note that the proposed error estimator is fundamentally based on the assumptions: $\lambda_i \approx \bar{\lambda}_i$ and $(\boldsymbol{\varphi})_i \approx (\bar{\boldsymbol{\varphi}})_i$. That is, the accuracy of the error estimator depends on the exact error value. In Ref. [23], it was investigated that, in numerical results, the estimation accuracy is quite good when the exact error is less than 0.1 (10% error). Hence, it is recommended to select an error tolerance level smaller than 0.1 for convincing the reliability of the error estimator.

For an additional investigation on this issue, we here further analyze $\delta\Pi(\bar{\lambda}_i)$ in Eq. (15c). The ith approximated eigenvector $(\bar{\boldsymbol{\varphi}})_i$ can be defined by a linear combination of the original eigenvectors [16,17,29]

$$(\bar{\boldsymbol{\varphi}})_i = \sum_{k=1}^{N} \alpha_k (\boldsymbol{\varphi})_k, \tag{21}$$

where α_k are coefficients for the linear combination.

When the approximated eigenvector is close enough to the original eigenvector, we can assume

$$\alpha_i \approx 1, |\alpha_i| \gg |\alpha_i - 1|, |\alpha_1|, |\alpha_2|, \ldots, |\alpha_{i-1}|, |\alpha_{i+1}|, \ldots, |\alpha_N|, \tag{22}$$

but, basically, values of α_k depend on how well the master DOFs are selected.

Substituting Eq. (21) into Eq. (13b), $(\delta\boldsymbol{\varphi})_i$ can be expressed by

$$(\delta\boldsymbol{\varphi})_i = (\boldsymbol{\varphi})_i - \sum_{k=1}^{N} \alpha_k (\boldsymbol{\varphi})_k, \tag{23}$$

in which the original eigenvectors $(\boldsymbol{\varphi})_i$ and $(\boldsymbol{\varphi})_k$ satisfy the mass-orthonormality and stiffness-orthogonality conditions: $(\boldsymbol{\varphi})_i^T \mathbf{M} (\boldsymbol{\varphi})_j = \delta_{ij}$ and $(\boldsymbol{\varphi})_i^T \mathbf{K} (\boldsymbol{\varphi})_j = \lambda_i \delta_{ij}$ with the Kronecker delta δ_{ij} ($\delta_{ij} = 1$ if $i = j$; otherwise, $\delta_{ij} = 0$).

Using Eq. (23) in Eq. (15c) and applying the mass-orthonormality and stiffness-orthogonality conditions, $\delta\, \Pi$ is represented by

$$\delta\, \Pi = \sum_{\substack{k=1 \\ k \neq i}}^{N} \alpha_k^2 \left(\frac{\lambda_k}{\lambda_i} - 1 \right), \tag{24}$$

where λ_i and λ_k are the original eigenvalues calculated from the original FE model. In Eq. (24), it is easily identified that $\delta\, \Pi$ is not only a master DOFs-dependent but also a problem-dependent quantity. That is, the reliability of the error estimator depends on how well the master DOFs are selected and dynamic characteristics of the original FE model.

When λ_c is a cut-off eigenvalue to select master DOFs, Guyan reduction is valid for $\lambda < \lambda_c$. In this validity domain, Guyan reduction gives well approximated eigensolutions. The proposed error estimator is derived for Guyan reduction using Kidder's approach, and both Guyan reduction and Kidder's approach are valid for $\lambda < \lambda_c \approx \sigma_1$ [24–26]. Therefore, the validity domain of the proposed error estimator is basically the same to that of Guyan reduction. However, due to the assumptions $\lambda_i \approx \bar{\lambda}_i$ and $(\boldsymbol{\varphi})_i \approx (\bar{\boldsymbol{\varphi}})_i$, the reliability of the proposed error estimator depends on the accuracy of eigensolutions approximated by Guyan reduction within the validity domain. Since lower modes are more accurately approximated in Guyan reduction, the proposed error estimator provides better accuracy for lower modes ($\lambda \ll \lambda_c$). The reliability of the proposed error estimator will be numerically studied in Section 5.4.

In addition, since λ_i is only an unknown variable in Eq. (17), we could correct $\bar{\lambda}_i$ using the relation: $\lambda_i \approx \bar{\lambda}_i/(1+\eta_i)$. This is a simple correction technique of the approximated eigenvalues. This point will be also discussed through numerical examples.

4. Simplified formulation of the error estimator

Although the error estimator in Eq. (18) is calculated by simple matrix additions and multiplications, it is difficult to handle when the FE model size is very large. Furthermore, the original formulation of the error estimator is relatively complicated. To handle this problem, we here propose a simplified formulation of the error estimator.

Expanding Eq. (18), the error estimator can be rewritten as

$$\begin{aligned} \eta_i = & -2(\boldsymbol{\varphi}_1)_i^T \mathbf{T}_G^T \mathbf{K} \mathbf{T}_r^{(1)} (\boldsymbol{\varphi}_1)_i + \bar{\lambda}_i (\boldsymbol{\varphi}_1)_i^T [2\mathbf{T}_G^T \mathbf{M} \mathbf{T}_r^{(1)} \\ & - 2\mathbf{T}_G^T \mathbf{K} \mathbf{T}_r^{(2)} - \mathbf{T}_r^{(1)T} \mathbf{K} \mathbf{T}_r^{(1)}] (\boldsymbol{\varphi}_1)_i + \Theta\left(\bar{\lambda}^2\right) + \Theta\left(\bar{\lambda}^3\right) + \Theta\left(\bar{\lambda}^4\right), \end{aligned} \tag{25}$$

and then, neglecting the higher order terms of $\bar{\lambda}$, the error estimator is approximated as the 0th and 1st order terms of $\bar{\lambda}$

$$\eta_i \approx -2(\boldsymbol{\varphi}_1)_i^T \mathbf{T}_G^T \mathbf{K} \mathbf{T}_r^{(1)} (\boldsymbol{\varphi}_1)_i + \bar{\lambda}_i (\boldsymbol{\varphi}_1)_i^T [2\mathbf{T}_G^T \mathbf{M} \mathbf{T}_r^{(1)} - 2\mathbf{T}_G^T \mathbf{K} \mathbf{T}_r^{(2)} - \mathbf{T}_r^{(1)T} \mathbf{K} \mathbf{T}_r^{(1)}] (\boldsymbol{\varphi}_1)_i. \tag{26}$$

Eq. (26) contains four matrices as $\mathbf{T}_G^T \mathbf{K} \mathbf{T}_r^{(1)}$, $\mathbf{T}_G^T \mathbf{M} \mathbf{T}_r^{(1)}$, $\mathbf{T}_G^T \mathbf{K} \mathbf{T}_r^{(2)}$ and $\mathbf{T}_r^{(1)T} \mathbf{K} \mathbf{T}_r^{(1)}$. Those matrices are specifically written in the component matrix level using Eqs. (2), (7) and (9), and then, the following relations are obtained

$$\mathbf{T}_G^T \mathbf{M} \mathbf{T}_r^{(1)} = \mathbf{T}_r^{(1)T} \mathbf{K} \mathbf{T}_r^{(1)}, \qquad \mathbf{T}_G^T \mathbf{K} \mathbf{T}_r^{(1)} = \mathbf{0}, \qquad \mathbf{T}_G^T \mathbf{K} \mathbf{T}_r^{(2)} = \mathbf{0}. \tag{27}$$

Consequently, using Eqs. (26) and (27), a new formulation of the error estimator, which is much simpler and more efficient than the original formulation, can be defined as

$$\eta_i \approx \bar{\lambda}_i (\boldsymbol{\varphi}_1)_i^T \mathbf{T}_r^{(1)T} \mathbf{K} \mathbf{T}_r^{(1)} (\boldsymbol{\varphi}_1)_i. \tag{28}$$

Eq. (28) is an approximated formulation of the original error estimator in Eq. (18), but its estimating accuracy might be almost the same as the original one because the insignificant higher order terms of $\bar{\lambda}$ in Eq. (18) are neglected.

To verify the computational efficiency of the proposed formulation in Eq. (28), we investigated its operation count theoretically, and also compared it with the count of the original formulation in Eq. (18). The computational costs of the original and present formulations are composed of default and incremental operations. In this paper, the default

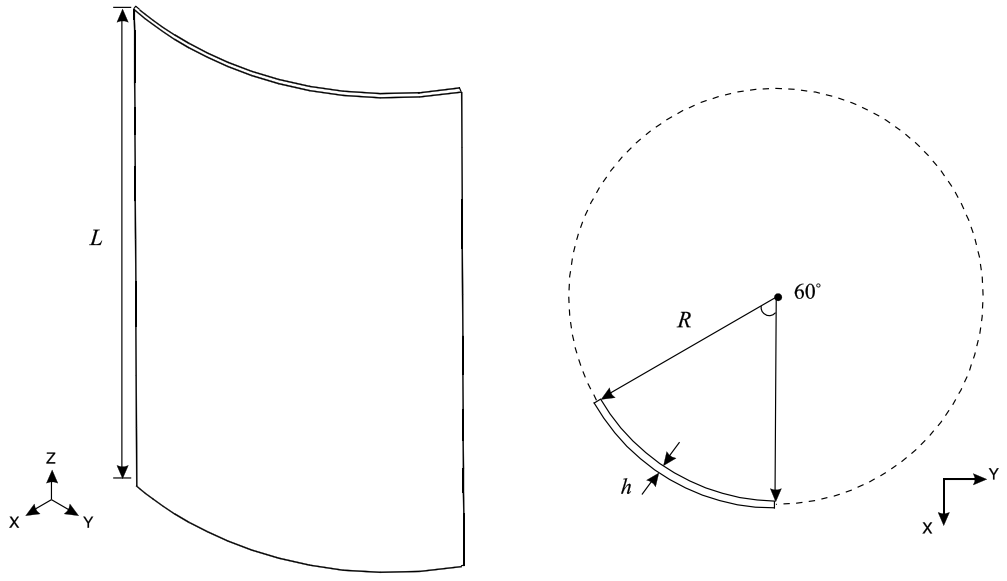

Fig. 1. Cylindrical panel problem.

Table 1
Comparison of the error estimators.

		Kim and Lee [23]	Present
Formulation		$(\boldsymbol{\varphi}_1)_i^T\,[2\mathbf{T}_G + \bar{\lambda}_i\,\mathbf{T}_r^{(1)} + \bar{\lambda}_i^2\,\mathbf{T}_r^{(2)}]^T$ $[\bar{\lambda}_i\mathbf{M} - \mathbf{K}]\,[\mathbf{T}_r^{(1)} + \bar{\lambda}_i\,\mathbf{T}_r^{(2)}](\boldsymbol{\varphi}_1)_i$	$\eta_i \approx \bar{\lambda}_i\,\boldsymbol{\chi}_i^T \cdot \boldsymbol{\psi}_i$ with $\boldsymbol{\chi}_i = \mathbf{T}_r^{(1)}(\boldsymbol{\varphi}_1)_i,\ \boldsymbol{\psi}_i = \mathbf{K}\,(\boldsymbol{\chi})_i.$
Operation counts	Default	$4(N_1N_2N + N_1^2N + 2N_1^2N_2)$	–
	Increment	$12n(N_1^2 + N_1 + 2)$	$n(N_2^2 + 2N_1N_2 + N_2 + 1)$

Table 2
Exact and estimated eigenvalue errors in the cylindrical panel problem.

Mode number	(a) Case of 59 nodes selected in uniform mesh			(b) Case of 41 nodes selected in distorted mesh		
	Exact	Estimated		Exact	Estimated	
		Kim and Lee [23]	Present		Kim and Lee [23]	Present
1	1.563E−04	1.563E−04	1.563E−04	1.177E−03	1.179E−03	1.174E−03
2	1.010E−03	1.012E−03	1.010E−03	7.285E−03	7.377E−03	7.220E−03
3	1.688E−03	1.691E−03	1.687E−03	1.225E−02	1.248E−02	1.202E−02
4	3.459E−03	3.471E−03	3.455E−03	1.216E−02	1.237E−02	1.202E−02
5	3.738E−03	3.752E−03	3.733E−03	1.187E−02	1.211E−02	1.182E−02
6	7.738E−03	7.801E−03	7.721E−03	4.010E−02	4.299E−02	3.751E−02
7	9.195E−03	9.283E−03	9.170E−03	6.055E−02	6.544E−02	5.414E−02
8	1.112E−02	1.124E−02	1.108E−02	6.082E−02	6.677E−02	5.593E−02
9	1.327E−02	1.344E−02	1.321E−02	5.382E−02	6.008E−02	5.146E−02
10	1.621E−02	1.649E−02	1.614E−02	7.150E−02	7.983E−02	6.791E−02
11	2.156E−02	2.202E−02	2.144E−02	1.982E−01	2.405E−01	1.580E−01
12	2.223E−02	2.272E−02	2.212E−02	1.276E−01	1.254E−01	9.024E−02
13	2.941E−02	3.032E−02	2.915E−02	1.055E−01	1.089E−01	1.173E−01
14	2.398E−02	2.455E−02	2.384E−02	8.867E−02	1.185E−01	9.334E−02

operation is the multiplication between known matrices, and its results are stored in memory. That is, $\mathbf{T}_r^{(1)T}\,\mathbf{K}\,\mathbf{T}_r^{(1)}$ in Eq. (28) is calculated at once and stored. In addition, since $\bar{\lambda}_i$ and $(\boldsymbol{\varphi}_1)_i$ are changed depending on global mode numbers, matrix–vector, vector–vector and scalar product operations are added in each global mode number, and it is defined as an incremental operation.

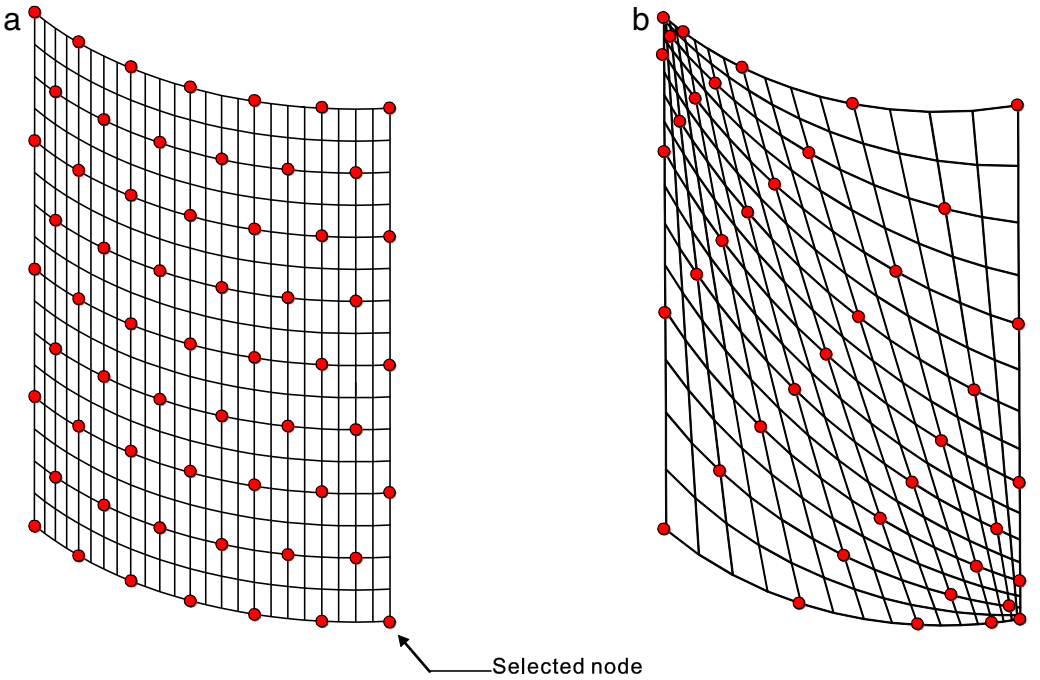

Fig. 2. Selected nodes in the cylindrical panel problem. (a) 59 nodes in uniform mesh and (b) 41 nodes in distorted mesh. At each selected node, all DOFs are considered as master DOFs.

Table 3
Computational costs of the error estimators in the cylindrical panel problem (59 nodes in uniform mesh, see Fig. 2(a)). 29 global modes are considered here ($n = 29$).

	Kim and Lee [23]	Present (using Eq. (29))
Operation count	6.634E+09	1.285E+08
Computing time	0.563704 s	0.011271 s

Table 4
Comparisons of eigenvalues in the cylindrical panel problem.

Mode number	(a) Case of 59 nodes selected in uniform mesh			(b) Case of 41 nodes selected in distorted mesh		
	λ_i Exact	$\bar{\lambda}_i/(1+\eta_i)$ Corrected	$\bar{\lambda}_i$ Approx.	λ_i Exact	$\bar{\lambda}_i/(1+\eta_i)$ Corrected	$\bar{\lambda}_i$ Approx.
1	6.154E+04	6.154E+04	6.155E+04	6.385E+04	6.385E+04	6.393E+04
2	3.727E+05	3.727E+05	3.730E+05	3.806E+05	3.807E+05	3.834E+05
3	5.904E+05	5.904E+05	5.914E+05	6.090E+05	6.092E+05	6.165E+05
4	1.218E+06	1.218E+06	1.222E+06	1.413E+06	1.413E+06	1.430E+06
5	1.250E+06	1.250E+06	1.255E+06	1.448E+06	1.448E+06	1.465E+06
6	2.970E+06	2.970E+06	2.993E+06	3.175E+06	3.183E+06	3.303E+06
7	3.359E+06	3.359E+06	3.390E+06	3.622E+06	3.644E+06	3.841E+06
8	3.912E+06	3.912E+06	3.956E+06	4.643E+06	4.665E+06	4.926E+06
9	4.530E+06	4.530E+06	4.590E+06	5.210E+06	5.222E+06	5.491E+06
10	6.495E+06	6.495E+06	6.600E+06	7.595E+06	7.620E+06	8.138E+06
11	9.470E+06	9.471E+06	9.674E+06	1.135E+07	1.174E+07	1.360E+07
12	1.024E+07	1.024E+07	1.047E+07	1.213E+07	1.255E+07	1.368E+07
13	1.190E+07	1.190E+07	1.225E+07	1.363E+07	1.349E+07	1.507E+07
14	1.244E+07	1.245E+07	1.274E+07	1.426E+07	1.420E+07	1.553E+07

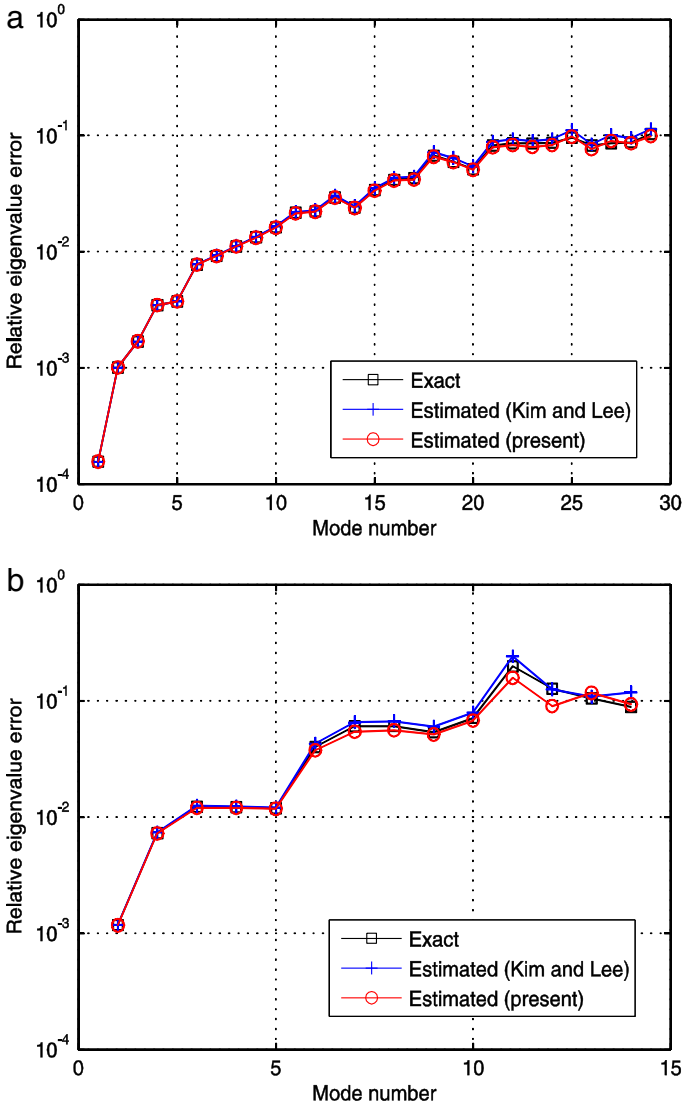

Fig. 3. Exact and estimated relative eigenvalue errors in the cylindrical panel problem. (a) 59 nodes selected in uniform mesh and (b) 41 nodes selected in distorted mesh.

$\mathbf{K}$ and $\mathbf{T}_r^{(1)}$ are $N \times N$ and $N \times N_1$ matrices, respectively. Hence, the matrix–matrix product operation of $\mathbf{K}\,\mathbf{T}_r^{(1)}$ is $N^2 N_1$ in general. However, since, in Eq. (9b), $\mathbf{T}_r^{(1)}$ has a $N_1 \times N_1$ block matrix with zero components, the operation count of $\mathbf{K}\,\mathbf{T}_r^{(1)}$ is reduced to $N_1 N_2 N$. Consequently, the operation count of $\mathbf{T}_r^{(1)T}\,\mathbf{K}\,\mathbf{T}_r^{(1)}$ that is the default operation of the present formulation in Eq. (28) is calculated by $N_1 N_2 N + N_1^2 N_2$. Similarly, the default operation count of the original formulation in Eq. (18) is also calculated by $4(N_1 N_2 N + N_1^2 N + 2N_1^2 N_2)$. This is more than four times larger than the default operation count of the present formulation.

In Eqs. (18) and (28), the default operations make $N_1 \times N_1$ matrices only. Hence, their matrix–vector and vector–vector product operation counts are N_1^2 and N_1, respectively. When we assume that the number of the global mode is n, the incremental operation counts in Eqs. (18) and (28) are calculated as $12n(N_1^2 + N_1 + 2)$ and $n(N_1^2 + N_1 + 1)$, respectively. It should be noted that N_1 is much smaller than N and N_2, and also that n might be smaller than N_1 in general. Therefore, the incremental operation count is not significant in the total computational cost. Considering those operation counts, we can conclude that the present error estimator is more efficient than the original error estimator.

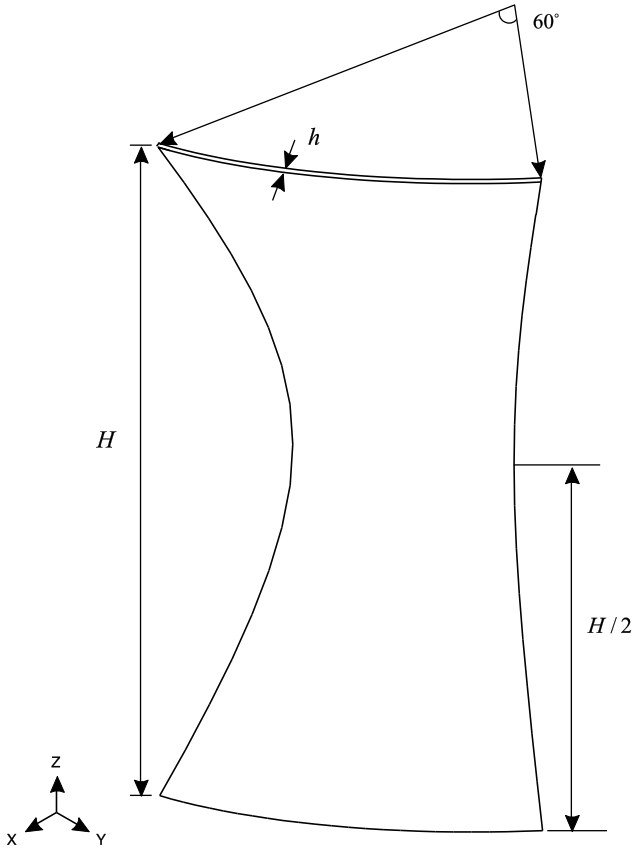

Fig. 4. Hyperboloid panel problem.

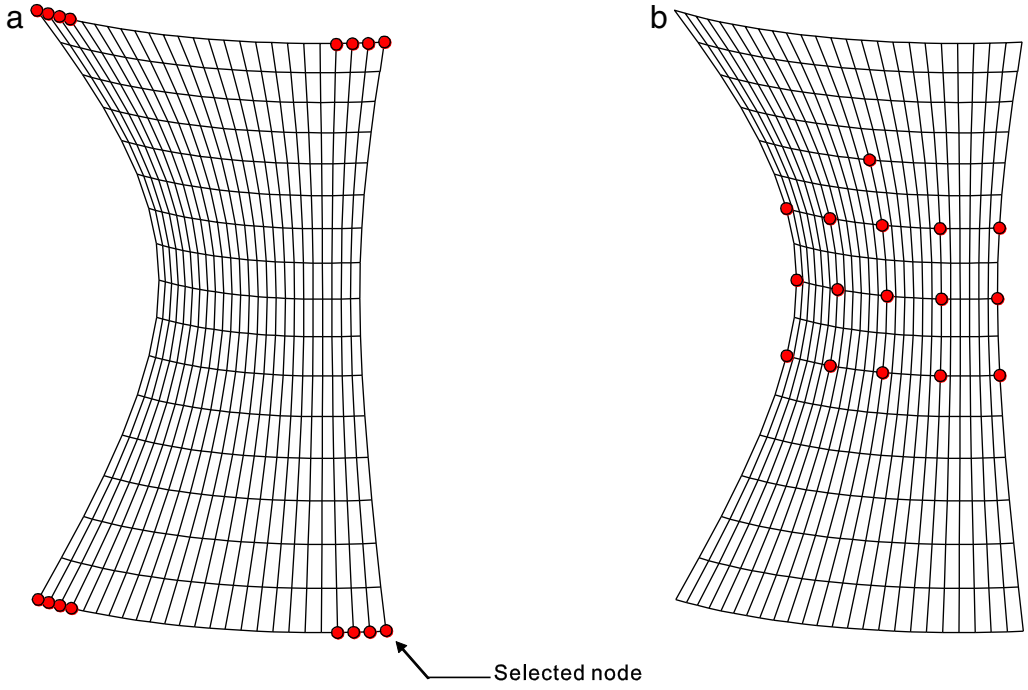

Fig. 5. Selected nodes in the hyperboloid panel problem. (a) 16 nodes selected by the DOFs selection criterion [24,25] and (b) 16 nodes selected badly. At each selected node, all DOFs are considered as master DOFs.

Table 5
Computational costs of the error estimators in the hyperboloid panel problem (16 nodes selected by the DOFs selection criterion, see Fig. 5(a)). 15 global modes are considered here ($n = 15$).

	Kim and Lee [23]	Present (using Eq. (29))
Operation count	1.551E+09	6.767E+07
Computation time	0.141025 s	0.006405 s

Table 6
Computational costs of the error estimators in the shaft–shaft interaction problem (39 nodes selected, see Fig. 10(a)). 20 global modes are considered here ($n = 20$).

	Kim and Lee [23]	Present (using Eq. (29))
Operation count	6.800E+09	2.447E+08
Computation time	0.580685 s	0.015101 s

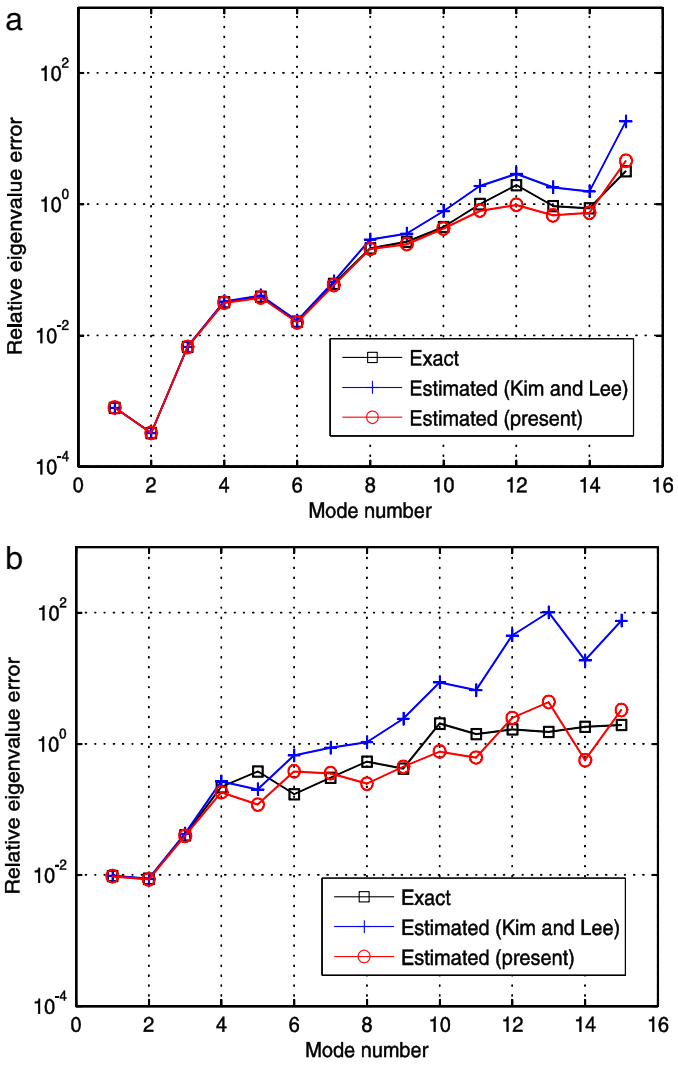

Fig. 6. Exact and estimated relative eigenvalue errors in the hyperboloid panel problem. (a) 16 nodes selected by the DOFs selection criterion [24,25] and (b) 16 nodes selected badly.

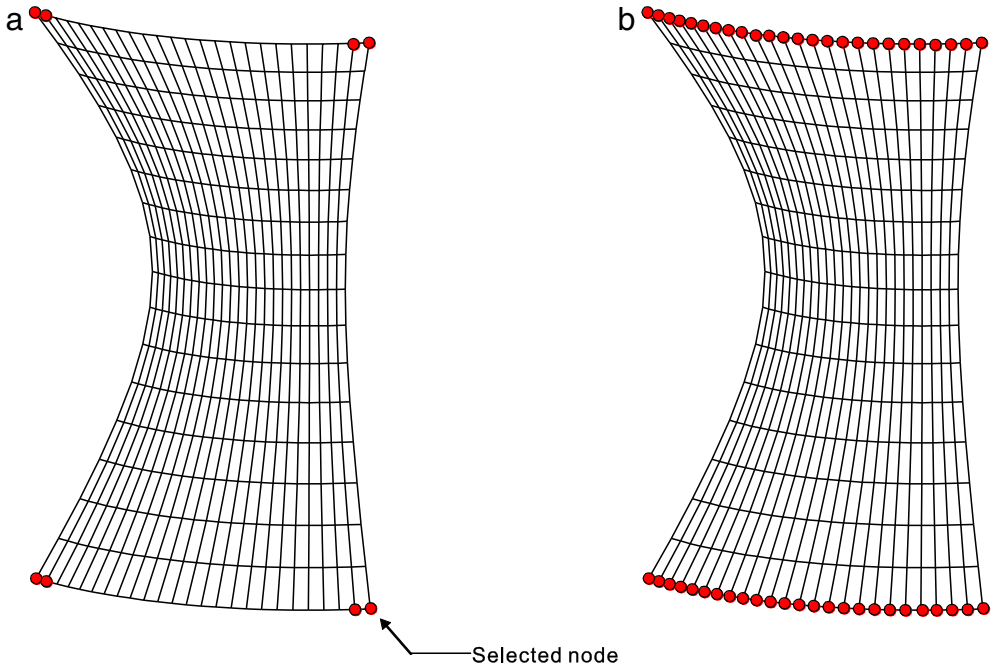

Fig. 7. Selected nodes in the hyperboloid panel problem. (a) 8 nodes selected when $f_c = 600$ Hz and (b) 50 nodes selected when $f_c = 1000$ Hz. At each selected node, all DOFs are considered as master DOFs.

In addition, for better computational efficiency of the proposed error estimator, Eq. (28) could be obtained using the vector operation as follows:

$$\eta_i \approx \bar{\lambda}_i \, \boldsymbol{\chi}_i^T \cdot \boldsymbol{\psi}_i \tag{29a}$$

with

$$\boldsymbol{\chi}_i = \mathbf{T}_r^{(1)} (\boldsymbol{\varphi}_1)_i, \qquad \boldsymbol{\psi}_i = \mathbf{K} \, (\boldsymbol{\chi})_i. \tag{29b}$$

Note that Eq. (29) does not have the default operation, and its total operation count (only the incremental operation count) is $n(N_2^2 + 2N_1N_2 + N_2 + 1)$. When n is not extremely large as is usual in engineering practice, Eq. (28) makes much smaller value than the total operation count of Eq. (28), $N_1N_2N + N_1^2N_2 + n(N_1^2 + N_1 + 1)$. Since the lower global modes, generally 10 to 40 modes, are only considered in engineering practice, Eq. (29) is quite reasonable to efficiently predict the exact error. The comparison of the original and present error estimators is presented in Table 1.

5. Numerical examples

In this section, we report the performance of the simplified error estimator, and we also compare it with the original error estimator. For the numerical study, we consider three shell structural problems: cylindrical panel, hyperboloid panel, and shaft–shaft interaction problems [30,31]. Specifically, the computational costs of the error estimators are explored. The operation counts are calculated using Table 1 based on the full matrix operation, and the computing time is obtained using MATLAB in a personal computer (Intel Core (TM) i7-4770, 3.40 GHz CPU, 16GB RAM).

5.1. Cylindrical panel problem

We here consider a cylindrical panel problem with free boundary condition, see Fig. 1. Length L is 0.8 m, radius R is 0.5 m, and thickness h is 0.005 m. Young's modulus E is 69 GPa, Poisson's ratio ν is 0.35, and density ρ is 2700 kg/m^3. Two numerical cases, with 59 nodes selected in a 24×16 uniform mesh ($N = 2125$), and 41 nodes in a 16×16 distorted mesh ($N = 1445$), are considered as shown in Fig. 2. Fig. 3 shows that the simplified error estimator also estimates well the exact relative eigenvalue error, as does the original error estimator. The exact and estimated

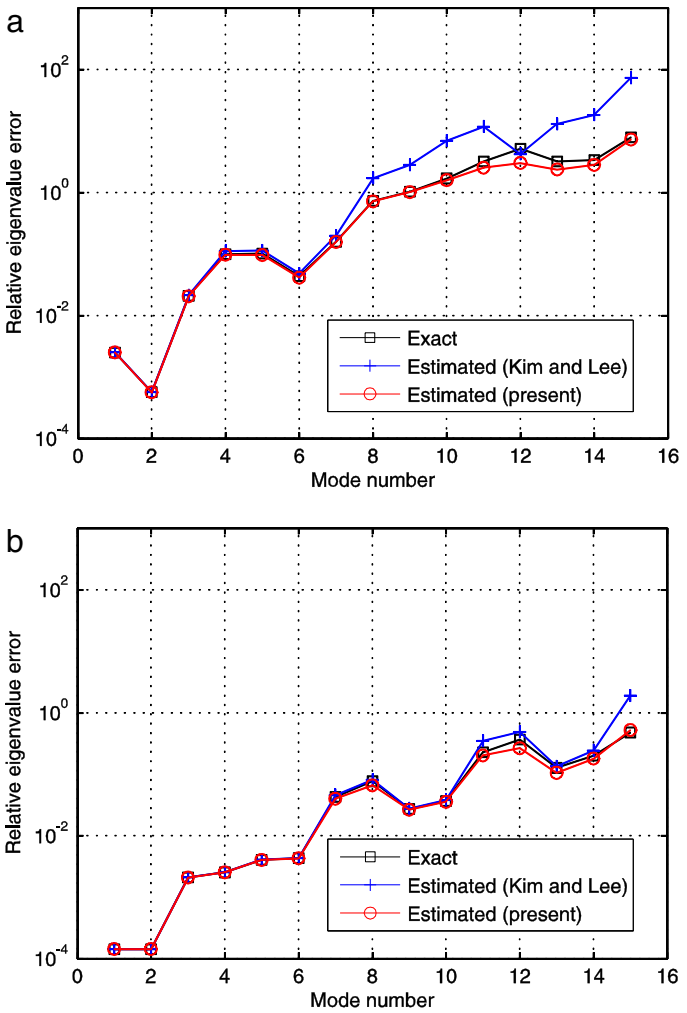

Fig. 8. Exact and estimated relative eigenvalue errors in the hyperboloid panel problem. (a) 8 nodes selected when $f_c = 600$ Hz and (b) 50 nodes selected when $f_c = 1000$ Hz.

relative eigenvalue errors are presented in Table 2. The total operation counts and computing times are also calculated in the first numerical case, and those details are presented in Table 3. The numerical result clearly shows the improved efficiency of the present error estimator.

We here examine a simple correction technique for the approximated eigenvalues using $\lambda_i \approx \bar{\lambda}_i/(1+\eta_i)$ derived from Eq. (17). Table 4 shows that the corrected eigenvalues are more accurate than the approximated eigenvalues $\bar{\lambda}_i$.

5.2. *Hyperboloid panel problem*

The estimating performance of the proposed error estimator is tested using a hyperboloid panel, see Fig. 4. No boundary condition is imposed. Height H and thickness h are 4 m and 0.005 m, respectively. Its mid-surface is defined by

$$x^2 + y^2 = 2 + z^2; \quad z \in [-2, 2]\,. \tag{30}$$

Its material properties are the same as with the cylindrical panel problem. It is modeled by a 24×16 mesh of shell finite elements ($N = 2125$).

To investigate the effect of the master DOFs selection, we here employ two different ways. First, a well-known DOFs selection criterion using the ratio of the diagonal terms of mass and stiffness matrices (K_{ii}/M_{ii}) is

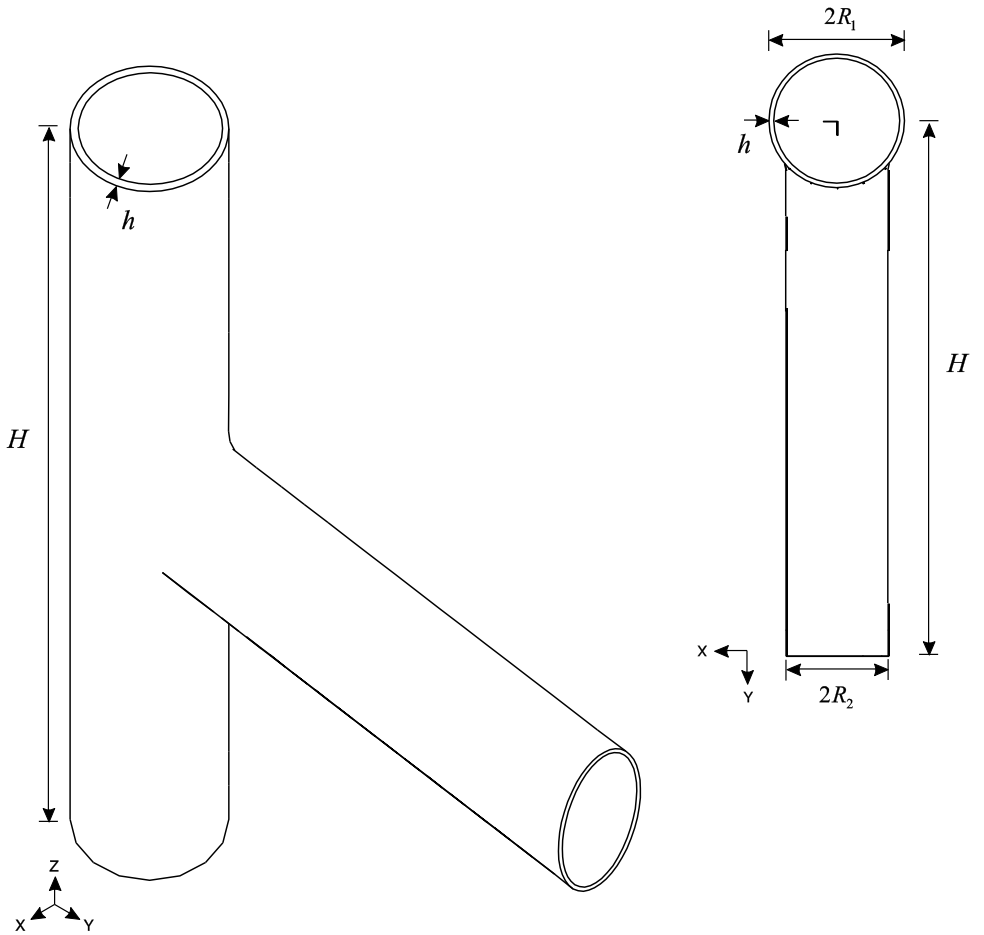

Fig. 9. Shaft–shaft interaction problem.

employed [32,33], see Fig. 5(a), and, to exemplify a badly selected case, the master nodes are arbitrarily selected as shown in Fig. 5(b). Only 16 master nodes ($N_1 = 80$) are selected in the two numerical cases.

When the master DOFs are selected well, both error estimators accurately estimate the exact error, see Fig. 6(a). However, when the master DOFs are badly selected, the present error estimator exhibits more accuracy than the original error estimator, see Fig. 6(b). Numerical results notably show that the error estimators are neither upper nor lower bounds of the exact error. In addition, in Table 5, the total computational costs of the first numerical case are specifically presented, and this directly implies the efficiency of the present error estimator.

In addition, we examine the performance of the error estimator by varying the cut-off frequency f_c, that is, varying the number of the master DOFs. We here consider $f_c = 600$ Hz and $f_c = 1000$ Hz, and then the master DOFs are selected as presented in Fig. 7. Numerical results show that the error estimation performance becomes more accurate in relatively higher global modes when the number of the master DOFs increases, see Fig. 8.

5.3. Shaft–shaft interaction problem

We here consider a complicated FE model that represents two connected cylindrical shafts with different radius ($R_1 = 0.0$ m and $R_2 = 0.0075$ m), see Fig. 9. Fillets, a radius 0.002 m, are used in the interface of two shafts, and no boundary condition was imposed. Height H and thickness h are 0.08 m and 0.0005 m, respectively. Young's modulus E is 207 GPa, Poisson's ratio ν is 0.29, and density ρ is 2700 kg/m^3. The model includes 555 nodes and 534 shell finite elements ($N = 2775$).

We consider two differently selected master DOFs (39 nodes and 70 nodes), see Fig. 10. The numerical results in Fig. 11 and Table 6 show that the proposed error estimator is accurate and efficient. In Fig. 12, we compare the

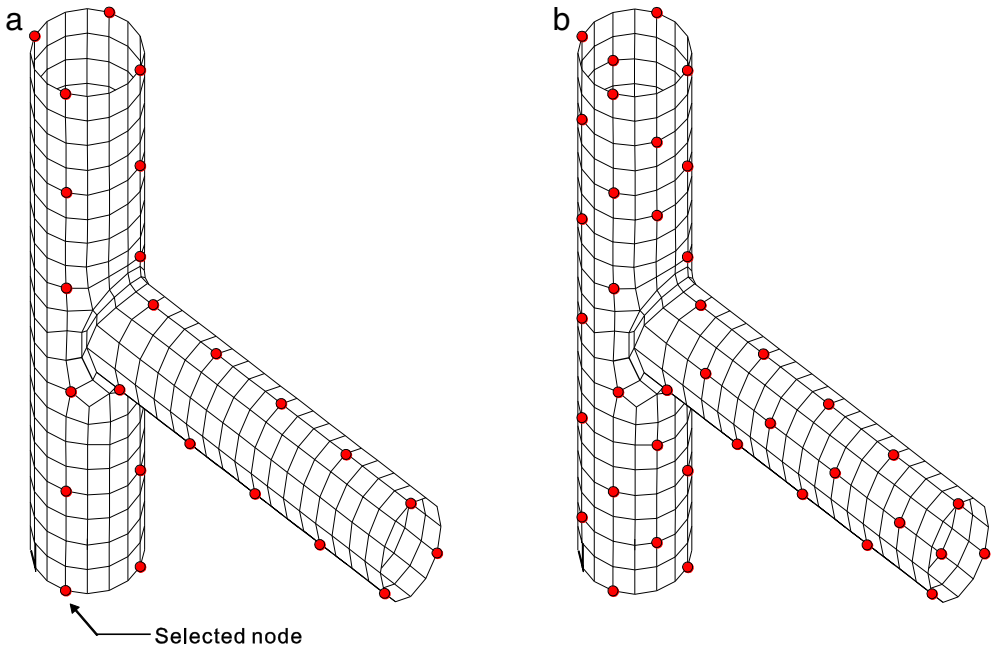

Fig. 10. Selected nodes of the shaft–shaft interaction problem. (a) 39 nodes and (b) 70 nodes. At each selected node, all DOFs are considered as master DOFs.

Table 7
Differences between the exact and estimated errors when $\xi_i \leq 0.1$ (10% error).

Case		σ_1	$\max(\bar{\lambda}_i)$ when $\xi_i \leq 0.1$	Mode number when $\max(\bar{\lambda}_i)$	$\max\left(\frac{\lvert\xi_i-\eta_i\rvert}{\xi_i}\right)$
Cylindrical panel	(a)	1.861E+08	5.034E+07	29	7.553E−02
	(b)	1.359E+07	7.595E+06	10	1.059E−01
Hyperboloid panel	(a)	2.201E+04	4.593E+03	7	4.826E−02
	(b)	3.914E+03	2.968E+02	3	2.222E−02
	(c)	8.297E+03	2.784E+03	6	5.948E−02
	(d)	3.147E+04	2.504E+04	10	1.376E−01
Shaft-shaft interaction	(a)	4.159E+10	1.443E+10	14	9.569E−02
	(b)	1.185E+11	3.085E+10	27	1.537E−01

computational efficiency of the present error estimator in Eqs. (28) and (29) varying the number of the interesting global mode denoted by n, and this shows that the total operation count of Eq. (29) with vector operation is not bigger than the one of Eq. (28) when n is smaller than 197.

5.4. On the reliability of the error estimator

Through various numerical examples considered in this study, it was observed that the exact error increases according to the global mode number. Then, the estimated errors are diverged from the exact errors. The basic assumptions of the proposed error estimator ($\lambda_i \approx \bar{\lambda}_i$ and $(\boldsymbol{\varphi})_i \approx (\bar{\boldsymbol{\varphi}})_i$) become poor when $\bar{\lambda}_i$ is close to σ_1 (that is, in relatively higher global modes).

To investigate the reliability of the error estimator, we consider exact and estimated relative eigenvalue errors obtained in all the numerical examples. Then, 733 data samples are plotted in Fig. 13. Table 7 summarizes the maximum relative error of the exact and estimated eigenvalue errors as $\max(|\xi_i - \eta_i|/\xi_i)$ and the inequality $\bar{\lambda}_i < \sigma_1$. Those numerical results show that the proposed error estimator works well when the exact error ξ_i is less than 0.1 (10% error).

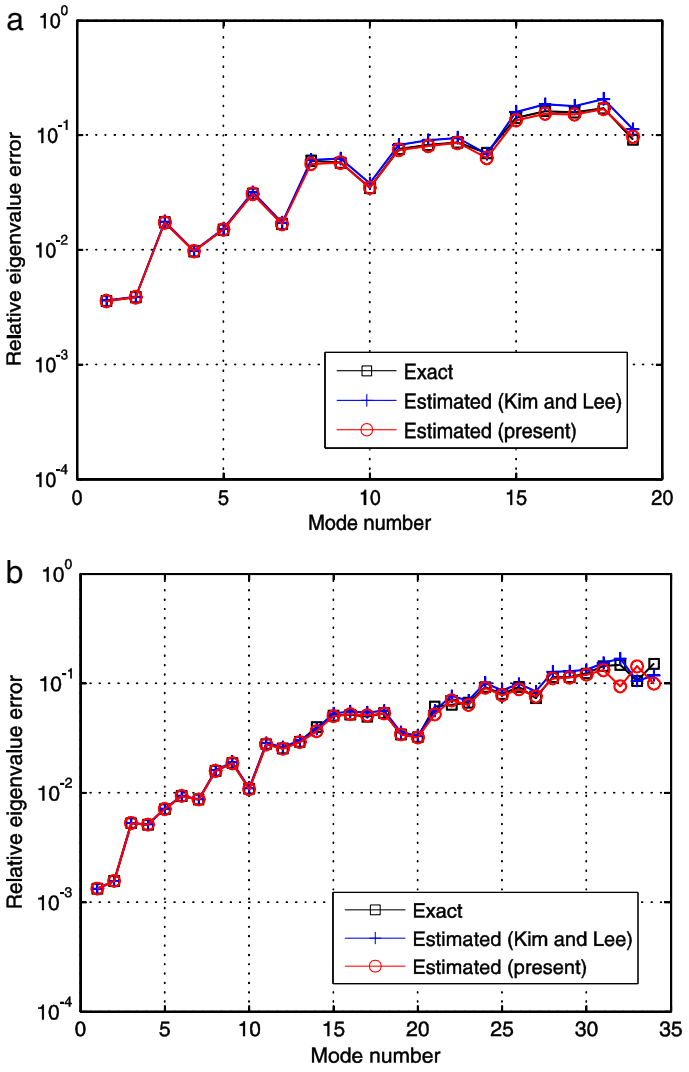

Fig. 11. Exact and estimated relative eigenvalue errors in the shaft–shaft interaction problem. (a) 39 nodes selected and (b) 70 nodes selected.

It is interesting to show the relation between ξ_i and $|\xi_i - \eta_i|$ using the least squares fitting

$$|\xi_i - \eta_i| = 0.2347\,(\xi_i)^{1.7339}\,, \tag{31}$$

and the coefficient of determination, R squared value, is close to 1 ($R^2 = 0.9049$), see Fig. 14.

6. Conclusions

Recently, we developed a novel error estimator for Guyan reduction to precisely predict the relative eigenvalue error [20]. Based on this work, we here propose a simplified formulation of the error estimator to improve its computational efficiency. The new formulation was developed from the original formulation by deriving the original formulation at the component matrix level and neglecting the higher order terms. The resulting formulation exhibits the same level of the estimating accuracy, but its computational cost is much cheaper than the original formulation. We here verified the estimating accuracy using various numerical examples, and also investigated its computational costs theoretically and numerically.

Due to the complicated formulation of the original error estimator [23], it is difficult to use for developing error estimators of the improved reduced system (IRS) method [5] and its iterative techniques (iE., the iterative IRS method

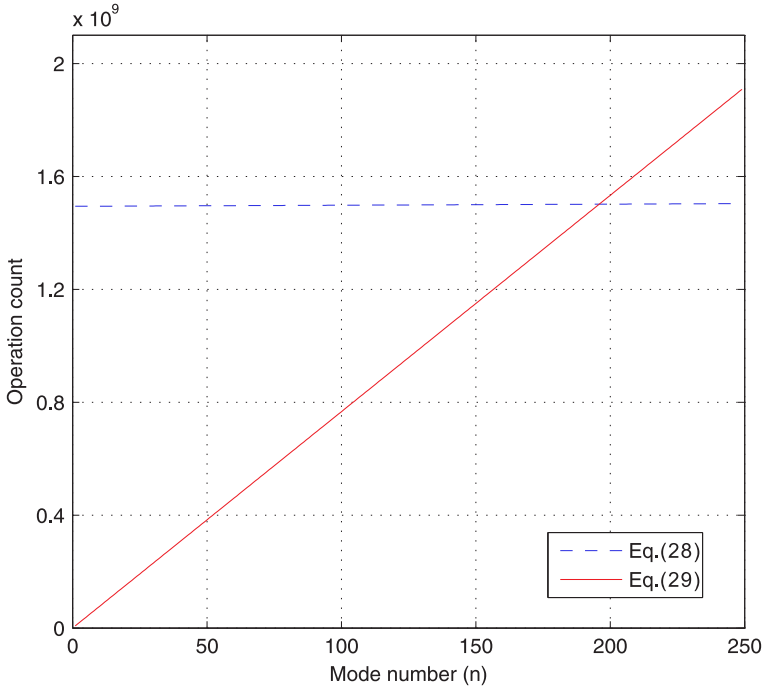

Fig. 12. Operation counts of Eqs. (28) and (29) in the shaft–shaft interaction problem (39 nodes selected).

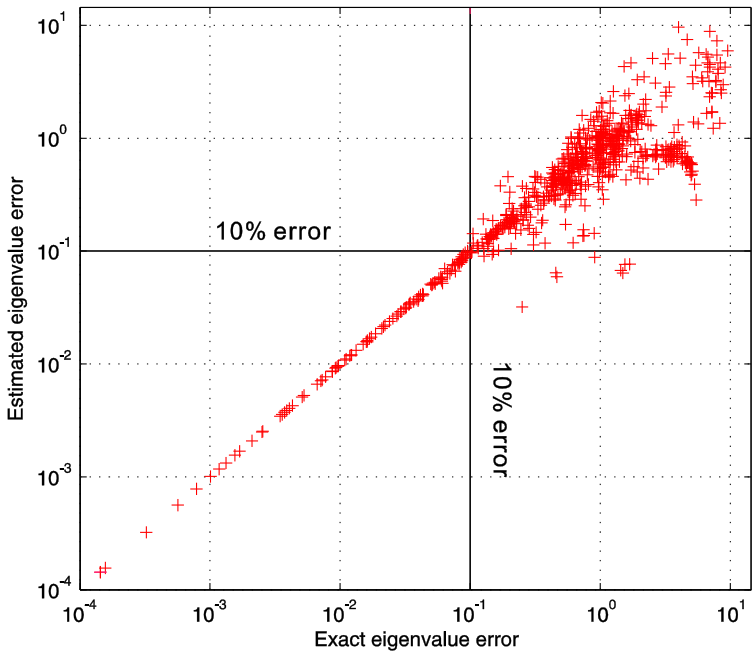

Fig. 13. Exact vs. estimated eigenvalue errors in all the numerical examples considered.

and the iterative order reduction (IOR) method [6–8,34]). However, the present work can give valuable insights to develop those error estimators, and also could be extended for the non-proportional damped system.

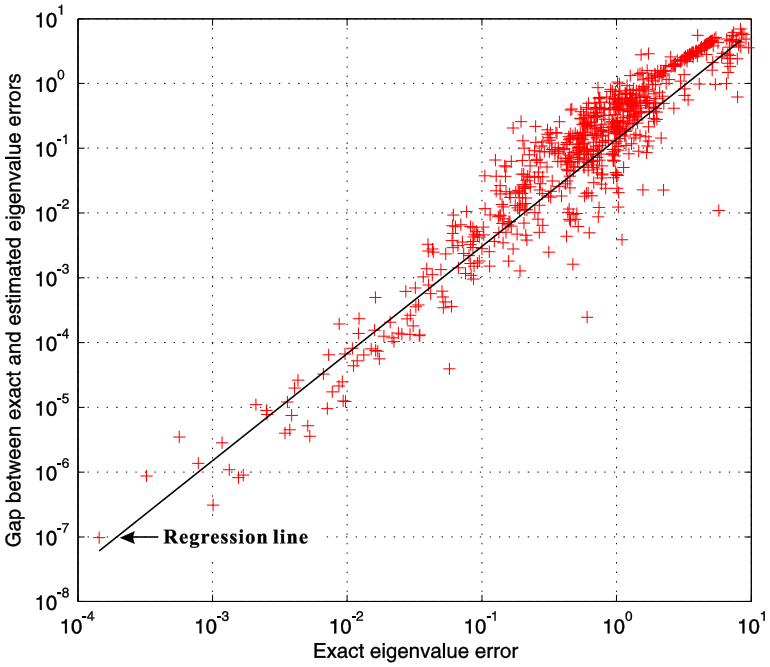

Fig. 14. Exact eigenvalue error vs. gap between the exact and estimated errors in all the numerical examples considered.

Acknowledgments

This work was supported by the Human Resources Development Program (No. 20134030200300) of the Korea Institute of Energy Technology Evaluation and Planning (KETEP) grant funded by the Korea government Ministry of Trade, Industry and Energy, and the Basic Science Research Programs through the National Research Foundation of Korea funded by the Ministry of Science, ICT, and Future Planning (No. 2014R1A2A2A01006497, No. 2015R1C1A1A01051499).

References

[1] R. Guyan, Reduction of stiffness and mass matrices, AIAA J. 3 (2) (1965) 380.
[2] B.M. Irons, Eigenvalue economisers in vibration problems, J. Roy. Aeronaut. Soc. 67 (1963) 526.
[3] R.L. Kidder, Reduction of structural frequency equations, AIAA J. 11 (6) (1973) 892.
[4] R.D. Henshell, J.H. Ong, Automatic masters from eigenvalues economization, Earthq. Eng. Struct. Dyn. 3 (1975) 375–383.
[5] J. O'Callanhan, A procedure for an improved reduced system (IRS) model, in: Proceeding the 7th International Modal Analysis Conference, Bethel, CT, 1989.
[6] M.I. Friswell, S.D. Garvey, JE.T. Penny, Model reduction using dynamic and iterated IRS techniques, J. Sound Vib. 186 (2) (1995) 311–323.
[7] Y. Xia, R. Lin, A new iterative order reduction (IOR) method for eigensolutions of large structures, Internat. J. Numer. Methods Engrg. 59 (2004) 153–172.
[8] D. Choi, H. Kim, M. Cho, Iterative method for dynamic condensation combined with substructuring scheme, J. Sound Vib. 317 (1–2) (2008) 199–218.
[9] H. Kim, M. Cho, Improvement of reduction method combined with sub-domain scheme in large-scale problem, Internat. J. Numer. Methods Engrg. 70 (2007) 206–251.
[10] W. Hurty, Dynamic analysis of structural systems using component modes, AIAA J. 3 (4) (1965) 678–685.
[11] R.R. Craig, B.C.C. Bampton, Coupling of substructures for dynamic analysis, AIAA J. 6 (7) (1968) 1313–1319.
[12] R.H. MacNeal, Hybrid method of component mode synthesis, Comput. Struct. 1 (4) (1971) 581–601.
[13] J.G. Kim, S.H. Boo, P.S. Lee, An enhanced AMLS method and its performance, Comput. Methods Appl. Mech. Engrg. 287 (2015) 90–111.
[14] J.G. Kim, P.S. Lee, An enhanced Craig–Bampton method, Internat. J. Numer. Methods Engrg. 103 (2015) 79–93.
[15] K.C. Park, J.G. Kim, P.S. Lee, A mode selection criterion based on flexibility approach in component mode synthesis, in: 53th AIAA/ASME/ASCE/AHS/ASC Structures, Structural Dynamics, and Materials Conference, Hawaii, USA, 2012.
[16] J.G. Kim, K.H. Lee, P.S. Lee, Estimating relative eigenvalue errors in the Craig–Bampton method, Comput. Struct. 139 (2014) 54–64.
[17] J.G. Kim, P.S. Lee, A posteriori error estimation method for the flexibility-based component mode synthesis, AIAA J. 53 (10) (2015) 2828–2837.

[18] J. Kim, J.G. Kim, G. Yun, P.S. Lee, D.N. Kim, Towards modular analysis of supramolecular protein assemblies, J. Chem. Theory Comput. 11 (2015) 4260–4272.
[19] J.G. Kim, S.H. Boo, P.S. Lee, Performance of the enhanced Craig–Bampton method, in: The 2015 World Congress on Advances in Structural Engineering and Mechanics, ASEM2015, Inchon, Korea, 2015.
[20] S.H. Boo, J.G. Kim, P.S. Lee, Simplified error estimator for the Craig–Bampton method and its application to error control, Comput. Struct. 164 (2016) 53–62.
[21] S.H. Boo, J.G. Kim, P.S. Lee, Error estimation for the automated multi-level substructuring method, Internat. J. Numer. Methods Engrg. http://dx.doi.org/10.1002/nme.5161 (in press).
[22] T.J.R. Hughes, The Finite Element Method: Linear Static and Dynamic Finite Element Analysis, Dover, Mineola, NY, USA, 2000.
[23] J.G. Kim, P.S. Lee, An accurate error estimator for Guyan reduction, Comput. Methods Appl. Mech. Engrg. 279 (2014) 1–19.
[24] K.B. Petersen, M.S. Pedersen, The Matrix Cookbook, Vol. 7, Technical University of Denmark, 2008, p. 15.
[25] R.L. Kidder, Reply by author to AH Flax, AIAA J. 13 (5) (1975) 702–703.
[26] V.N. Shah, M. Raymund, Analytical selection of masters for the reduced eigenvalue problem, Internat. J. Numer. Methods Engrg. 18 (1) (1982) 89–98.
[27] L. Meirovitch, Elements of Vibration Analysis, McGraw-Hill, 1975.
[28] L. Meirovitch, H. Baruh, On the inclusion principle for the hierarchical finite element method, Internat. J. Numer. Methods Engrg. 19 (2) (1983) 281–291.
[29] K.J. Bathe, Finite Element Procedures, Klaus-Jürgen Bathe, 2006.
[30] Y. Lee, P.S. Lee, K.J. Bathe, The MITC3+ shell finite element and its performance, Comput. Struct. 138 (2014) 12–23.
[31] Y. Lee, H.M. Jeon, P.S. Lee, K.J. Bathe, The modal behavior of the MITC3+ triangular shell element, Comput. Struct. 153 (2015) 148–164.
[32] R.D. Henshell, J.H. Ong, Automatic masters from eigenvalues economization, Earthq. Eng. Struct. Dyn. 3 (1975) 375–383.
[33] J.H. Ong, Improved automatic masters for eigenvalues economization, Finite Elem. Anal. Des. 3 (2) (1987) 149–160.
[34] J.G. Kim, P.S. Lee, K.C. Park, A model selection algorithm for the flexibility-based component mode synthesis, in: 5th International Conference on Computational Methods in Structural Dynamics and Earthquake Engineering, Crete, Greece, 2015.